OPEN ACCESS Freely available online

PLOS ONE

Fabrication of Smart Chemical Sensors Based on Transition-Doped-Semiconductor Nanostructure Materials with μ-Chips

Mohammed M. Rahman[1,2]*, Sher Bahadar Khan[1,2], Abdullah M. Asiri[1,2]

1 Center of Excellence for Advanced Materials Research, King Abdulaziz University, Jeddah, Saudi Arabia, **2** Chemistry Department, Faculty of Science, King Abdulaziz University, Jeddah, Saudi Arabia

Abstract

Transition metal doped semiconductor nanostructure materials (Sb_2O_3 doped ZnO microflowers, MFs) are deposited onto tiny μ-chip (surface area, ~0.02217 cm^2) to fabricate a smart chemical sensor for toxic ethanol in phosphate buffer solution (0.1 M PBS). The fabricated chemi-sensor is also exhibited higher sensitivity, large-dynamic concentration ranges, long-term stability, and improved electrochemical performances towards ethanol. The calibration plot is linear ($r^2 = 0.9989$) over the large ethanol concentration ranges (0.17 mM to 0.85 M). The sensitivity and detection limit is ~5.845 $\mu A cm^{-2} mM^{-1}$ and ~0.11±0.02 mM (signal-to-noise ratio, at a SNR of 3) respectively. Here, doped MFs are prepared by a wet-chemical process using reducing agents in alkaline medium, which characterized by UV/vis., FT-IR, Raman, X-ray photoelectron spectroscopy (XPS), powder X-ray diffraction (XRD), and field-emission scanning electron microscopy (FE-SEM) etc. The fabricated ethanol chemical sensor using Sb_2O_3-ZnO MFs is simple, reliable, low-sample volume (<70.0 μL), easy of integration, high sensitivity, and excellent stability for the fabrication of efficient I–V sensors on μ-chips.

Citation: Rahman MM, Khan SB, Asiri AM (2014) Fabrication of Smart Chemical Sensors Based on Transition-Doped-Semiconductor Nanostructure Materials with μ-Chips. PLoS ONE 9(1): e85036. doi:10.1371/journal.pone.0085036

Editor: Suresh Bhargava, RMIT University, Australia

Received June 20, 2013; **Accepted** November 23, 2013; **Published** January 13, 2014

Funding: This work was funded by the Deanship of Scientific Research (DSR), King Abdulaziz University, Jeddah, under grant No. 130-019-D1433. The authors, therefore, acknowledge with thanks DSR technical and financial support. The funders had no role in study design, data collection and analysis, decision to publish, or preparation of the manuscript.

Competing Interests: The authors have declared that no competing interests exist.

* E-mail: mmrahman@kau.edu.sa

Introduction

The development of chemi-sensors has been the subject of considerable interest in recent years based on μ-chips using specific matrixes. Such modification on μ-chip offers great attention to chemical detection that included high-sensitivity, inherent-miniaturization, low-cost, high selectivity, low-sample volume, independence of sample turbidity or optical-path length, minimal-power demands, and high bio-compatibility with advanced microfabrication technologies. The development of electrochemical chemi-sensors for sensitive detection of toxic chemicals is generally required innovative approaches that coupled with various modification/amplification procedures onto electro-active substrates. Semiconductor codoped materials have attracted much interest because of their unique properties and potential applications in all areas of advance science and technological fields [1]. The simplest synthetic route for doped-materials is possibly self-aggregation, in which ordered doped aggregates are prepared in economical approaches [2]. Although, it is still a big-challenge to develop simple and economical route for microstructures semiconductor codoped metal oxide with designed chemical components and controlled morphologies, which is strongly influenced the optical and electrical properties of doped nanomaterials [3]. The significance of safety for human-beings and environments has been considered with great attention in doped semiconductor chemi-sensors for toxic chemical detection (toxic level in human blood, >0.10% or 2.2 mM) by reliable methods using μ-chips [4,5]. Semiconductor micro-structure materials are very sensitive due to their particle-size and high-active surface-area as compared to the transition materials in micro-ranges. Nanoscale materials composed micro-structures have also displayed a huge-deal of consideration due to their promising properties such as large active-surface area, high-stability, quantum confinement, high-porosity, and permeability (meso-porous nature), which is directly dependent on the shape and size of the microcrystals [6,7]. During the last two decades, semiconductor nanomaterials have been received significant attention due to their electronic, magnetic, electrical, optoelectronic, mechanical properties, and their prospective applications in nanotechnology fields. Doped materials might be a promising candidate because of their high-specific surface-area, low-resistance, fascinating electrochemical, and optical properties [8,9]. Solution–liquid–solid mechanism [10], vapor–solid mechanism [11], and oxide-assisted growth mechanism [12] have also been adopted to prepare various antimony oxide nanostructure materials. Recently, antimony oxide nanostructure have been also prepared using micro-emulsion [13] and templating CNTs [14] by several groups, however, nanosheets composed microstructure of Sb_2O_3-doped ZnO MFs have never reported. In this report, it is displayed an alternative approach to the synthesis of Sb_2O_3-ZnO MFs with diameters of several nanometers sheet composed several micrometers flowers by a wet-chemical process. Here, semiconductor zinc oxide (ZnO, band-gap ~3.4 eV, II–VI compound, binding energy ~60 meV,

excellent acoustic wave, and n-type semiconductor) has been recognized as a promising host material at room conditions, which displayed a wurtzite type structure with number of periodic planes with hexagonally-coordinated O and Zn atoms piled along the c-axis [15]. For outstanding and extraordinary properties of ZnO, it is used for flexible applications in piezo-electric chips, opto-electronics, photo-catalytic, solar cells, transparent thin- film transistors, bio- and chemi-sensors, spintronics, light-emitters, electronics, catalysis, and so forth [16–18]. For exotic and flexible properties including bio-compatibility, non-toxicity, chemical and photo-chemical stability, high-specific surface area, optical and electro-chemical behaviors, and high-electron communication characteristics, the transition-doped semiconductor nanomaterials presents itself as one of the most promising materials for the development and fabrication of efficient chemi-sensors [19,20]. Recently, the extensive progresses have been explored on ZnO-based nanomaterials synthesis by a wet-chemical and conventional techniques [21]. Zinc oxide nanostructure displayed attractive applications, such as transistors, UV photo-detectors, gas-sensors, field-emission electron sources, nano-wires and nano-lasers, nano-scale power generators, and many other functional devices [22–27].

Advances in nanotechnology for innovative chemi-sensors, nanomaterials embedded μ-chips have been regulating a key-task in the fabrication and improvement of very precise, perceptive, accurate, sensitive, and consistent sensors. The exploration for even tiny chips accomplished in nano-level imaging and controlling of doped nanomaterial for biological, chemical, pathological samples, chemi-sensor has recently expanded the spotlight of awareness of scientist mainly for control monitoring due to the amplifying essential for environmental safety and health monitoring [28,29]. Transition-doped semiconductor metal oxides are the model materials for sensing due to high-active surface areas and extensively employed as sensor for the detection, recognition, and quantification of various toxic pollutants and hazardous chemicals [30–34]. In presence of ethanol, it causes damage of brain and specific diseases of stomach, liver, and erythrocyte. Therefore it is important and big challenge to sense ethanol efficiently and shield the human health from dangerous diseases and safe the environment using electro-analytical methods [35]. Recently, a large amount of undoped metal oxides is considered as chemical sensors for the detection of different hazardous pollutants and toxic chemicals [36,37]. Therefore Sb_2O_3-ZnO MFs have been offered as a mediator to detect and quantify the ethanol chemicals in liquid phase. The main attention of the present investigation is to fabricate and develop a highly sensitive chemi-sensor (especially ethanol) for detecting and quantifying hazardous pollutants using Sb_2O_3-ZnO MFs on μ-chips. Hence a well-crystalline Sb_2O_3-ZnO MFs were prepared by a wet-chemical process and totally characterized by using UV/visible, FT-IR spectroscopy, XRD, FESEM, and XPS analysis etc.

In this contribution, it is prepared by a wet-chemical process to arrange as-prepared Sb_2O_3 doped ZnO MFs with practically controlled flower-shape structures, which exposed a control-morphological development in microstructure materials and potential chemi-sensor applications using tiny μ-chips. With most of the significant properties of the doped material, there have been more and more attention focused to explore the doped counter-parts. For semiconductor materials, doping is an exceptional function to improve significantly the optical and electrical properties, which enhances the development of electronic and opto-electronic devices. Codoped nanosheets composed Sb_2O_3-ZnO MFs are used to fabricate by a simple hydrothermal method on a tiny μ-chip surfaces, which allows very sensitive transduction of liquid/surface interactions and measured the chemical sensing performance considering ethanol at ambient conditions. To best of our knowledge, this is the first report for detection of toxic ethanol with as-grown Sb_2O_3-ZnO MFs onto tiny μ-chips using reliable I-V method in short response time.

Experimental Sections

Materials and Methods

Zinc chloride, butyl carbitol acetate, antimony chloride, ethyl acetate, ammonia solution (25%), and all other chemicals were in analytical grade and purchased from Sigma-Aldrich Company. They were used without further purification. The λ_{max} (289.0 nm) of as-grown Sb_2O_3 doped ZnO MFs was executed using UV/visible spectroscopy Lamda-950, Perkin Elmer, Germany. FT-IR spectra of MFs were measured on a spectrum-100 FT-IR spectrophotometer in the mid-IR range purchased from Bruker (ALPHA, USA). The XPS measurements of MFs were executed on a Thermo Scientific K-Alpha KA1066 spectrometer (Germany). Monochromatic AlK_α x-ray radiation sources were used as excitation sources, where beam-spot size was kept in 300.0 μm. The spectrum was recorded in the fixed analyzer transmission mode (pass energy, ~200.0 eV), where the sample scanning of the spectra was performed less 10^{-8} Torr. Morphology, size, elemental, and structure evaluation of as-grown MFs were recorded on FE-SEM instrument from JEOL (JSM-7600F, Japan). The powder XRD patterns of MFs were recorded by X-ray diffractometer from PANalytical diffractometer equipped with Cu-$K_{\alpha 1}$ radiation ($\lambda = 1.5406$ nm). The generator voltage (~45.0 kV) and generator current (~40.0 mA) were applied for the XRD measurement. Raman spectrometer was used to measure the Raman shift of as-grown MFs using radiation source (Ar^+ laser line, λ; 513.4 nm), which was purchased from Perkin Elmer (Raman station 400, Perkin Elmer, Germany). I–V technique (two electrodes composed on μ-chip) is measured by using Keithley-Electrometer from USA.

Preparation and growth mechanism of Sb_2O_3 doped ZnO MFs

Large-scale synthesis of Sb_2O_3-ZnO MFs was prepared by a wet-chemical process at low-temperature using zinc chloride ($ZnCl_2$), antimony chloride ($SbCl_3$), and ammonium hydroxide (NH_4OH). In a usual reaction process, 0.1 M $ZnCl_2$ dissolved in 50.0 ml deionized (DI) water mixed with 50.0 ml DI solution of 0.1 M $SbCl_3$ and 50.0 ml of 0.1 M urea under continuous stirring. The pH of the solution was adjusted to 9.7 by addition of NH_4OH and resulting mixture was shacked and stirred continuously for 30.0 minutes at room conditions. After stirring, the solution mixture was then put into conical flux and heat-up at 160°C for 12.0 hours. The temperature of solution was controlled manually throughout the reaction process at 90.0°C. After heating the reactant mixtures, the flux was kept for cooling at room conditions until reached to room temperature. The final codoped products were obtained, which was washed thoroughly with DI water, ethanol, and acetone for several times subsequently and dried at room-temperature for structural, elemental, morphological, and optical characterizations. The growth mechanism of the Sb_2O_3-ZnO nanostructure materials can be explained on the basis of chemical reactions and nucleation as well as growth of doped nanocrystals. The probable reaction mechanisms are presented here for attaining the codoped nanomaterial oxides in below.

$$\mathbf{NH_4OH_{(aq)} \rightarrow 2NH_4^+(aq) + OH_{(aq)}^-} \quad (\mathbf{i})$$

$$SbCl_3 + 3NH_4OH_{(aq)} + H_2O_{(aq)} \rightarrow Sb(OH)_{3aq)} + 3NH_4Cl + 2H_2O_{(aq)} \quad \text{(ii)}$$

$$ZnCl_{2(s)} + 2NH_4OH_{(aq)} \rightarrow Zn(OH)_{2(aq)} + 2NH_{4(aq)}^{+} + 2Cl_{(aq)}^{-} \quad \text{(iii)}$$

$$Zn(OH)_{2(aq)} + 4NH_4OH_{(aq)} + Sb(OH)_{3(aq)} \rightarrow Sb_2O_3.ZnO_{(s)} + 4NH_4^{+} + 2Cl^{-} + H_2O \quad \text{(iv)}$$

The reaction is forwarded slowly according to the proposed equation (i) to equation (iii). During preparation, the pH value of the reaction medium plays an important responsibility in the doped nano-material oxide formation. At a particular pH, when $SbCl_3$ is hydrolyzed with ammonia solution, antimony hydroxide is formed instantly according to the equation (ii). During the whole synthesis route, NH_4OH operates a pH buffer to control the pH value of the solution and slow contribute of hydroxyl ions (OH^-). When the concentrations of the Sb^{3+} and OH^- ions are achieved above in critical value, the precipitation of Sb_2O_3 nuclei begin to start. As there is high concentration of Zn^{2+} ions in the solution [according to the reactions (iii)], the nucleation of Sb_2O_3 crystals become slower due to the lower activation energy barrier of heterogeneous nucleation. Hence, as the concentration of Zn^{2+} existences, a number of larger Sb_2O_3.ZnO crystals with aggregated nanosheets composed flower-like morphology form after the reactions [equation (v)]. The shape of calcined Sb_2O_3.ZnO MFs is approximately reliable with the growth pattern of antimony doped zinc oxides crystals [38–40]. Then the solution was washed thoroughly with acetone, ethanol, and water consecutively and kept for drying at room condition. Finally, the as-grown doped Sb_2O_3.ZnO MFs nanomaterials were calcined at 400.0°C for 6 hours in the furnace (Barnstead Thermolyne, 6000 Furnace, USA). The calcined MFs were characterized in detail in terms of their morphological, structural, optical properties, and applied for ethanol chemical sensing based on μ-chips for the first time.

Fabrication and detection technique of ethanol using Sb_2O_3-ZnO MFs on μ-chips

The sensing area of μ-chip is fabricated with as-grown Sb_2O_3 doped ZnO MFs using butyl carbitol acetate (BCA) and ethyl acetate (EA) as a conducting coating agent by drop-coating method. Then it is put into oven at 60.0°C for two hours until the film is completely dry. 0.1 M phosphate buffer solution (PBS) at pH 7.0 is made by mixing 0.2 M Na_2HPO_4 and 0.2 M NaH_2PO_4 solution in 100.0 mL de-ionize water. A cell is consisted of Sb_2O_3-ZnO MFs fabricated μ-chip as a working and Pt connector is used a counter electrodes. As received ethanol is diluted to make various concentrations (0.17 mM to 8.5 M) in PBS solution and used as a target analyte. 70.0 μL of 0.17 mM PBS solution is kept constant during measurements onto the μ-chip. The ratio of current versus concentration (slope of calibration curve) is used to calculate of target ethanol chemical sensitivity. Limit of detection (LOD) is calculated from the ratio of 3N/S versus sensitivity (ratio of noise×3 vs. sensitivity) in the linear dynamic ranges of calibration plot. Electrometer is used as a voltage sources for I–V measurement in simple two electrodes μ-chip system. The as-grown Sb_2O_3-ZnO MFs are fabricated and employed for the detection of target analyte.

Results and Discussion

Optical properties of Sb_2O_3 doped ZnO MFs

The optical property of the as-grown Sb_2O_3 doped ZnO MFs is one of the significant characteristics for the assessment of its photo-catalytic activity. UV/visible absorption is a technique in which the outer electrons of atoms or molecules absorb radiant energy and undergo transitions to high energy levels. In this phenomenon, the spectrum obtained due to optical absorption can be analyzed to acquire the energy band-gap of the doped metal oxides. For UV/visible spectroscopy, the absorption spectrum of Sb_2O_3-ZnO MFs solution is measured as a function of wavelength, which is presented in Figure 1A. It presents a broad absorption band around 289.0 nm in the visible-range between 200.0 to 800.0 nm wavelengths indicating the formation of Sb_2O_3-ZnO MFs. Band-gap energy (E_{bg}) is calculated on the basis of the maximum absorption band of Sb_2O_3-ZnO MFs and found to be ~4.2907 eV, according to following equation (v).

$$Ebg = \frac{1240}{\lambda} \quad (\text{eV}) \qquad \text{(v)}$$

Where E_{bg} is the band-gap energy and λ_{max} is the wavelength (289.0 nm) of the Sb_2O_3-ZnO MFs. No extra peak associated with impurities and structural defects are observed in the spectrums, which proved that the synthesized microstructure controlled crystallinity of as-grown Sb_2O_3-ZnO MFs [41,42].

The as-grown Sb_2O_3 doped ZnO MFs is also investigated in terms of the atomic and molecular vibrations. To predict the functional-recognition, FT-IR spectra fundamentally in the region of 400~4000 cm^{-1} is investigated at room conditions. Figure 1B displays the FT-IR spectrum of MFs, which represents band at 489, 513, 1497, 1623, and 3408 cm^{-1}. These observed broad vibration bands (at 489 & 513 cm^{-1}) could be assigned as metal-oxygen (Sb-O & Zn-O mode) stretching vibrations, which demonstrated the configuration of Sb_2O_3-ZnO MF materials. The supplementary vibrational bands may be assigned to O-H bending vibration, C-O absorption, and O-H stretching. The

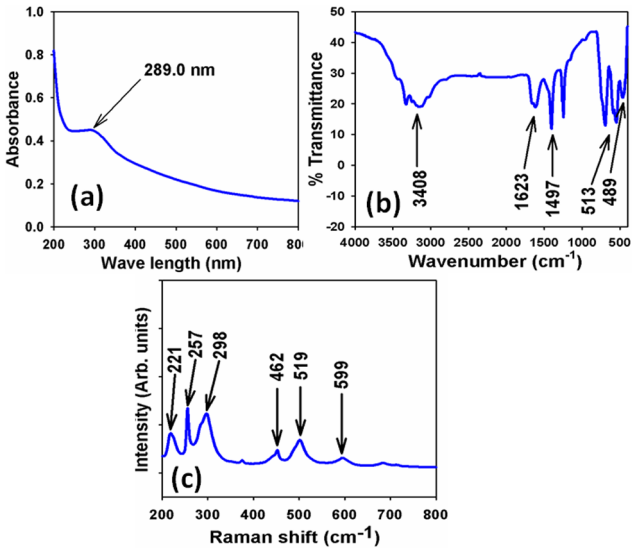

Figure 1. (a) UV/visible, (b) FT-IR, and (c) Raman spectroscopy of as-grown Sb_2O_3 doped ZnO MFs at room conditions.
doi:10.1371/journal.pone.0085036.g001

absorption bands at 1497, 1623, and 3408 cm^{-1} generally shows from CO_2 and water, which usually semiconductor doped nanostructure materials absorbed from the environment due to their high surface-to-volume ratio of mesoporous nature [43,44]. Finally, the experimental vibration bands at low frequencies regions recommended the formation of Sb_2O_3-ZnO MFs by a facile wet-chemical method. Raman spectroscopy is a spectroscopic technique utilized to display vibrational, rotational, and other low-frequency phases in a Raman active compound. It depends on inelastic scattering of monochromatic light (Raman scattering), usually from a laser in the visible, near infra-red, or near ultra-violet range. The laser light relates with molecular vibrations, phonons or other excitation in the modes, showing in the energy of the laser photons being shifted up or down. The shift in energy represents the information regarding the phonon modes in the system, where infrared spectroscopy yields similar, but complementary information. Raman spectroscopy is generally established and utilized in material chemistry, since the information is specific to the chemical bonds and symmetry of metal-oxygen stretching or vibrational modes. Usually, there are three vibration modes in Sb_2O_3-ZnO MFs nanomaterial crystal: A_1, E_1 and E_2, of which A_1 and E_1 split into longitudinal (A_{1L}, E_{1L}) and transverse (A_{1T}, E_{1T}) ones and E_2 contains low and high frequency phonons (E_{2L} and E_{2H}) [45,46]. As-grown Sb_2O_3-ZnO MFs is significantly altered the Raman spectra as well as the crystal of ZnO nanostructure [47,48]. Here, Figure 1c confirms the Raman spectrum, where key aspects of the wave number are employed at about 221, 298, and 257 cm^{-1} for metal-oxygen (Sb-O and Zn-O) stretching vibrations. The large bands can be assigned to a cubic phase of Sb_2O_3-ZnO MFs. At 462, 519, and 599 cm^{-1} higher wave-number shifts are revealed owing to the different dimensional effects of the MFs.

Morphological, Structural, and Elemental properties of Sb_2O_3 doped ZnO MFs

FE-SEM images of as-grown Sb_2O_3 doped ZnO MFs structures are presented in Figure 2(a–d). It exhibits the images of the MFs with micro-dimensional sizes of as-grown Sb_2O_3-ZnO MFs. The dimension of MF is calculated in the range of 2.4 μm, which composed of nanosheets (~65.0±10.0 nm). It is clearly exposed from the FE-SEM images that the facile synthesized Sb_2O_3-ZnO MFs is microstructures in flower-shape, which is grown in very high-density and possessing almost uniform nanosheet composed MFs. When the size of doped material decreases into micrometer-sized scale, the surface area is increased significantly, this improved the energy of the system and made re-distribution of Zn and Sb ions possible. The micrometer-sized flower could have tightly packed into the lattice, which is an agreement with the publish reports [49,50]. Crystallinity and crystal phase of Sb_2O_3-ZnO MFs were investigated using by powder X-ray diffractometer. Powder X-ray diffraction patterns of doped MFs are represented in Figure 2e. The Sb_2O_3.ZnO MFs were investigated and exhibited as face-centered cubic shapes. Figure 2e reveals characteristic crystallinity of the codoped Sb_2O_3.ZnO MFs and their crystalline arrangement, which is investigated using powder X-ray crystallography. All the reflection peaks in this prototype were related with ZnO phase having face-centered cubic zincite geometry [JCPDS # 071-6424]. The phases demonstrated the key features with indices for crystalline ZnO at 2θ values of 32.3(001), 39.8(002), 54.7(020), and 73.2(221) degrees. The face-centered cubic lattice parameters are a = 3.2494, b = 5.2038, and radiation ($CuK_\alpha 1$, λ = 1.5406). The ZnO phases have a high degree of crystallinity. All of the peaks match well with Bragg reflections of the standard zincite structure (point or space-group P63mc) [51–53]. The reflected peaks were also found to correspond with Sb_2O_3 phase having face-centered cubic orthorhombic geometry [JCPDS # 074-1725]. The phases demonstrated the key features with indices for crystalline Sb_2O_3 at 2θ values of 25.7(110), 28.1(111), 32.3(131), 43.6(002), 46.2(242), 59.2(052), 58.3(133), 60.3(072), and 67.4(341) degrees. The Sb_2O_3 phases have a high degree of crystallinity. All of the peaks match well with Bragg reflections of the standard orthorhombic structure. These confirmed that there is major number and amount of crystalline codoped Sb_2O_3-ZnO present in MFs [54].

X-ray photoelectron spectroscopy (XPS) is a quantitative spectroscopic method that determines the chemical-states of the elements that present within doped materials. XPS spectra are acquired by irradiating on a nanomaterial with a beam of X-rays, while simultaneously determining the kinetic energy and number of electrons that get-away from the top one to ten nm of the material being analyzed. Here, XPS measurements were measured for Sb_2O_3-ZnO MFs semiconductor nanomaterials to investigate the chemical states of ZnO and Sb_2O_3. The XPS spectra of Sb3d, Zn2p, and O1s are presented in Fig. 3a. XPS was also used to resolve the chemical state of the doped Sb_2O_3 nanomaterial and their depth. Figure 3b presents the XPS spectra (spin orbit doublet peaks) of the $Sb3d_{(3/2)}$ and $Sb3d_{(1/2)}$ regions recorded with semiconductor doped materials. The binding energy of the $Sb3d_{(3/2)}$ and $Sb3d_{(1/2)}$ peak at 529.1 eV and 539.6 eV respectively denotes the presence of Sb_2O_3 since their bindings energies are similar [55]. The O1s spectrum shows a main peak at 531.2 eV in Fig. 3c. The peak at 531.2 eV is

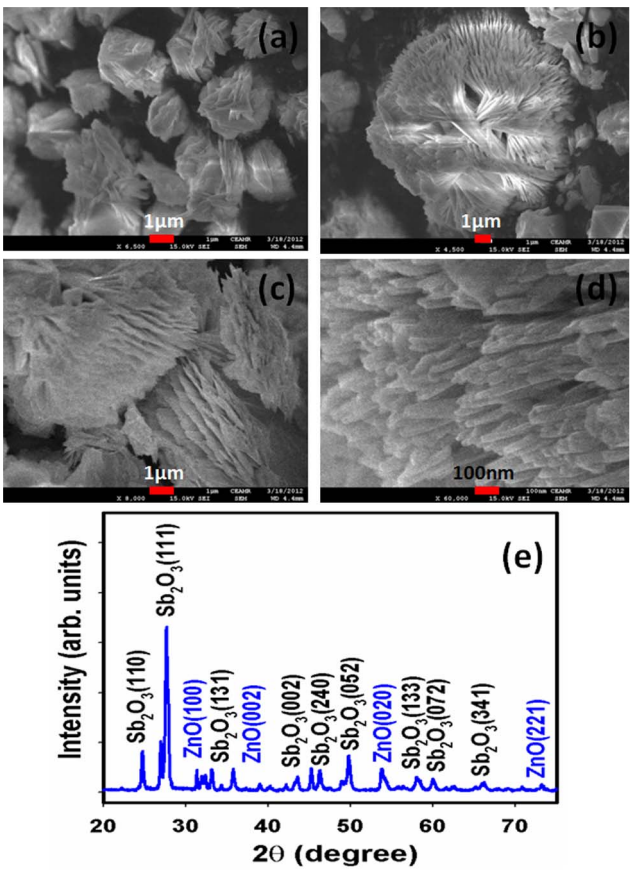

Figure 2. (a–d) FE-SEM images and (e) Powder x-ray diffraction pattern, of as-grown Sb_2O_3-ZnO MFs at room conditions.
doi:10.1371/journal.pone.0085036.g002

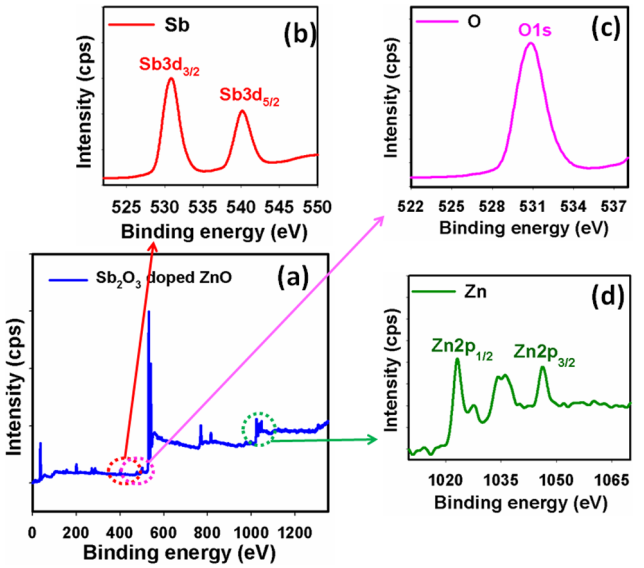

Figure 3. XPS of (a) doped Sb_2O_3-ZnO MFs, (b) Sb3d level, (c) O1s level, and (d) Zn2p level acquired with MgKα1 radiation.
doi:10.1371/journal.pone.0085036.g003

assigned to lattice oxygen may be indicated to oxygen (ie, O_2^-) presence in the doped Sb_2O_3-ZnO MF nanomaterials [56]. In Figure 3d, the spin orbit peaks of the $Zn2p_{(1/2)}$ and $Zn2p_{(3/2)}$ binding energy for all the samples appeared at around 1025 eV and 1048 eV respectively, which is in good agreement with the reference data for ZnO [57].

Preparation of μ-Chips using photolithography method

Electrochemical μ-chips were fabricated by conventional photolithographic technique, where electrodes and passivation layers are developed on silicon wafer followed by dicing and packaging [58]. Nitrogen-doped silicon wafers are prepared and overflowed by extra-pure water. In this step, all contaminations on the surface and native SiO_2 layer are removed perfectly. At first, the wet oxidation is employed and then dry oxidation is executed, where, wafers are annealed in the nitrogen environment. Aluminum is sputtered with aluminum-1% Si target. Then the photolithograph processes are applied. Resist coating, baking, exposure, and development are employed by Kanto chemicals, and then it is rinsed thoroughly by ionic water. Aluminum is etched by etching solution and resistance layer is removed perfectly by plasma etching instrument. Then silicon wafers are cleaned by acetone, methanol, and finally by plasma simultaneously. Silicon nitride (SiN) layer is deposited by chemical vapor deposition and then pad electrode surfaces are etched by reactive ion etching. Finally residual resist layer is removed by plasma etching. After photolithographic process, platinum is sputtered by SP150-HTS. Then it is patterned by lift-off method, in which wafers are immersed into the remover, and then washed with isopropyl alcohol. Photolithographic process is again investigated, where titanium is sputtered as a binding layer, and then gold is evaporated by deposition method. Finally, gold layer is patterned by lift-off method. Palylene passivation layer is formed for the protection of the μ-chip from water. Photolithographic process is performed again for pad protection. Then palylene-dimer is evaporated by deposition apparatus. Photolithography process is done again for patterning. Palylene layer is patterned by etching. Finally, un-necessary resists are removed by acetone and then wafer is cleaned by isopropyl alcohol (IPA). Resist is coated on a whole surface of the silicon wafer for protection during dicing process is executed. Silicon wafer is diced into pieces by dicing apparatus and stored into the desiccators, when not in use. Resist on μ-chip surface is removed by acetone and cleaned with isopropyl alcohol (IPA). The opposite side of the chip is roughed by a sandpaper sheet for better adhesion and electrical stability. The μ-chip is bonded with die and packaged by silver paste. It is dried in a drying oven. Pads on chip are connected to the package through gold wire with bonding machine. Finally, silicon-based adhesive is put on the periphery of the chip to protect pads and gold wire from sample solution. Adhesive is dried for 24 hours at room temperature. The semiconductor smart μ-chips were fabricated on silicon wafer. Aluminum was sputtered to fabricate as wiring and bonding pads. Pt-Ti-TiN was sputtered on thermal oxide of silicon and patterned by photolithography to fabricate counter electrode (CE). Ti-TiN layers were used for strong adhesion. Au-Ti were sputtered and lithographed, which made circular working electrode (WE) with a diameter of 1.68 mm in the center of the μ-chip. After electrodes fabrication, palylene layer was fabricated by evaporation method as a passivation layer. The wafer was diced to 5.0 mm square μ-chips. This μ-chip was bonded to a package by silver paste. Aluminum pads were connected to the package by gold wire. Finally, adhesive (Araldite, Hantsman, Japan) was put on the periphery of the chip, which prevents target solution from contacting pads (Figure 4a). The magnified construction view of internal μ-chip center (sensing area) is presented in the Figure 4(b–c).

Fabrication and chemical sensor application of Sb_2O_3-ZnO/μ-Chips assembly

The potential application of Sb_2O_3-ZnO MFs assembled onto μ-chip as chemical sensors (especially ethanol analyte) has been evaluated for measuring and detecting hazardous chemicals, which are not environmental affable. Improvement of doping of these nanosheets composed Sb_2O_3-ZnO MFs on μ-chip as chemical sensors is in the initial stage and no other reports are available. The MFs of Sb_2O_3-ZnO sensors have advantages such as stability in air, non-toxicity, chemical inertness, electrochemical activity, simplicity to assemble or fabrication, and bio-safe characteristics. As in the case of toxic ethanol sensors, the phenomenon of reason is that the current response in I-V method of Sb_2O_3-ZnO MFs considerably changes when aqueous ethanol are adsorbed. The calcined Sb_2O_3-ZnO MFs were applied for modification of chemical sensor, where ethanol was measured as target analyte. The fabricated-surface of Sb_2O_3-ZnO MFs sensor was made with conducting binders (EC & BCA) on the μ-chip surface, which is presented in the Figure 4(c–d). The fabricated μ-chip electrode was placed into the oven at low temperature (50.0°C) for 2 hours to make it dry, stable, and uniform the surface totally. I–V signals of chemical sensor are anticipated having Sb_2O_3-ZnO doped thin film as a function of current versus potential for hazardous ethanol. The real electrical responses of target ethanol are investigated by simple and reliable I–V technique using Sb_2O_3-ZnO MFs fabricated μ-chip, which is presented in Figure 4e.The time holding of electrometer was set for 1.0 sec. A significant amplification in the current response with applied potential is noticeably confirmed. The simple, reliable, possible reaction mechanism is generalized in Scheme 1d in presence of ethanol on Sb_2O_3-ZnO MFs sensor surfaces by I–V technique. The ethanol is converted to water and carbon dioxide in presence of doped nanomaterials by releasing electrons ($-6e^-$) to the reaction system (conduction band, C.B.), which improved and

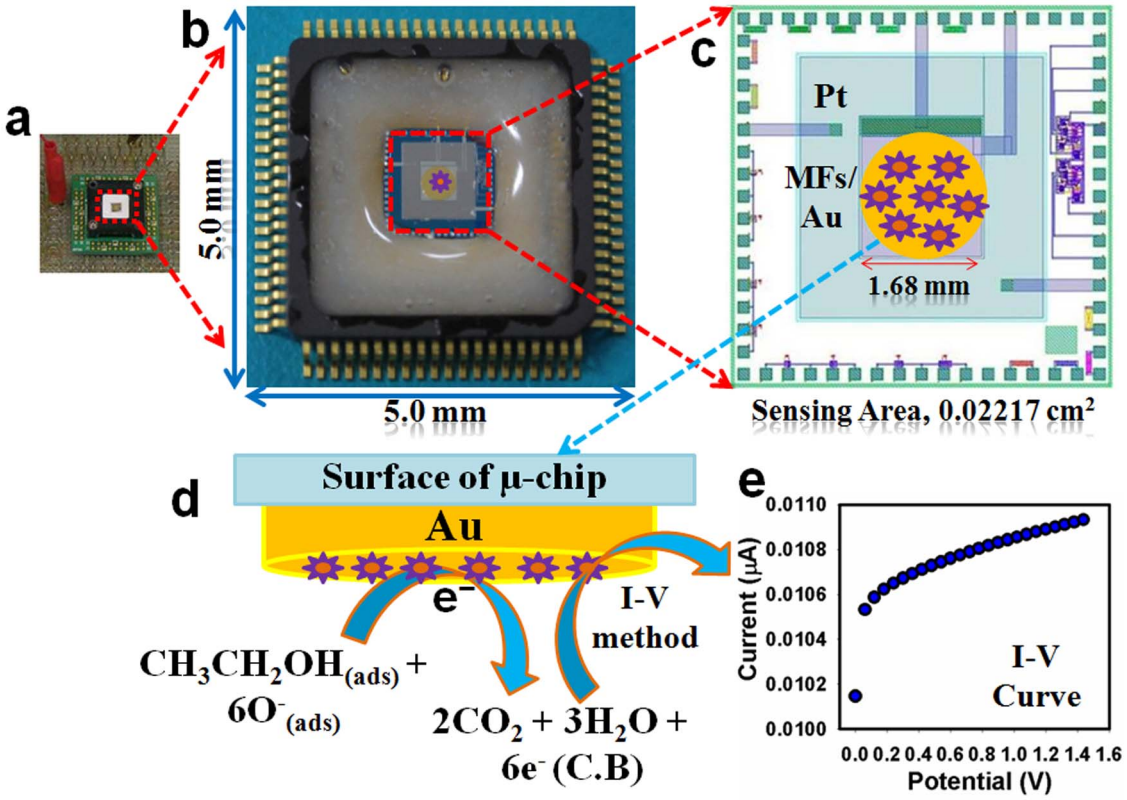

Figure 4. Schematic diagram of (a) real camera-view from top, (b) magnified view of μ-chip, (c) fabrication with Sb_2O_3-ZnO MFs with conducting binders (EC & BCA) onto μ-chip sensing-area, (d) reaction mechanism of ethanol in presence of doped Sb_2O_3-ZnO MFs, and (e) outcomes of I-V experimental results.
doi:10.1371/journal.pone.0085036.g004

enhanced the current responses against potential during the I–V measurement at room conditions.

Figure 5a shows the current responses of un-coated (gray-dotted) and coated (dark-dotted) μ-chip working electrodes with Sb_2O_3-ZnO MFs in absence of target ethanol. With nanosheets composed MFs fabricating surface, the current signal is slightly reduced compared to uncoated μ-chip surface, which indicates the surface is slightly blocked with doped MF nanomaterials in the buffer system. The current changes for the un-coated μ-chips (dark-dotted) towards target ethanol (~50.0 μL), and MF nanomaterials modified film before (deep-blue-dotted) and after (light-blue-dotted) injecting of target 50.0 μL ethanol (~0.17 mM) onto Sb_2O_3-ZnO MFs modified μ-chips is showed in Figure 5b. A significant current enhancement is exhibited with the Sb_2O_3-ZnO MFs modified μ-chips compared with uncoated μ-chips due to the presence of micro-structures, which has higher-specific surface area, larger-surface coverage, excellent absorption and adsorption capability into the porous MF surfaces towards the target ethanol. This significant change of surface current is examined in every injection of the target ethanol onto the doped modified μ-chips by electrometer. I–V responses with doped Sb_2O_3-ZnO MFs modified μ-chip surface are investigated from the various concentrations (0.17 mM to 8.5 M) of ethanol, which is showed in Figure 5c. It shows the current changes of fabricated μ-chip films as a function of ethanol concentration in room condition. It was also found that at low to high concentration of target analyte, the current responses were enhanced regularly. The potential current changes at lower to higher potential range (potential, + 0.10 V to +1.3 V) based on various analyte concentration are observed, which is clearly presented in Figure 5c. A large range of analyte concentration is measured the probable analytical limit, which is calculated in 0.17 mM to 8.5 M. The calibration (at + 0.3V) and magnified-calibration curves are plotted from the various ethanol concentrations, which are presented in the Figure 5(d–e). The sensitivity is estimated from the calibration curve, which is close to ~5.848 $\mu Acm^{-2}mM^{-1}$. The linear dynamic range of this sensor displays from 0.17 mM to 0.85 M (linearity, R = 0.9989) and the detection limit was considered as 0.11±0.001 mM [3×noise (N)/slope(S)].

Usually, the resistance value of doped semiconductor materials are decreased with increasing surrounding active oxygen, which is the fundamental characteristics of nanomaterials [59]. Actually, oxygen adsorption demonstrates an significant responsibility in the electrical properties of the Sb_2O_3-ZnO MFs onto μ-chip. The oxygen ion adsorption is removed the conduction electrons and increased the resistance of Sb_2O_3-ZnO MFs. Unstable oxygen species (i.e., O_2^- & O^-) are adsorbed on the doped MF surface at room temperature, and the quantity of such chemisorbed oxygen species is directly depended on morphological and structural properties. At room condition, O_2^- is chemisorbed, while on nanosheets composed microflowers morphology, O_2^- and O^- are chemisorbed significantly. For this reason, the active O_2^- is disappeared quickly [60]. Here, ethanol sensing mechanism on Sb_2O_3-ZnO MFs/μ-chip sensor is executed due to the presence of semiconductors oxides. The oxidation or reduction of the semiconductor MFs is held, according to the dissolved O_2 in bulk-solution or surface-air of the neighboring atmosphere according to the following equations (vi–viii).

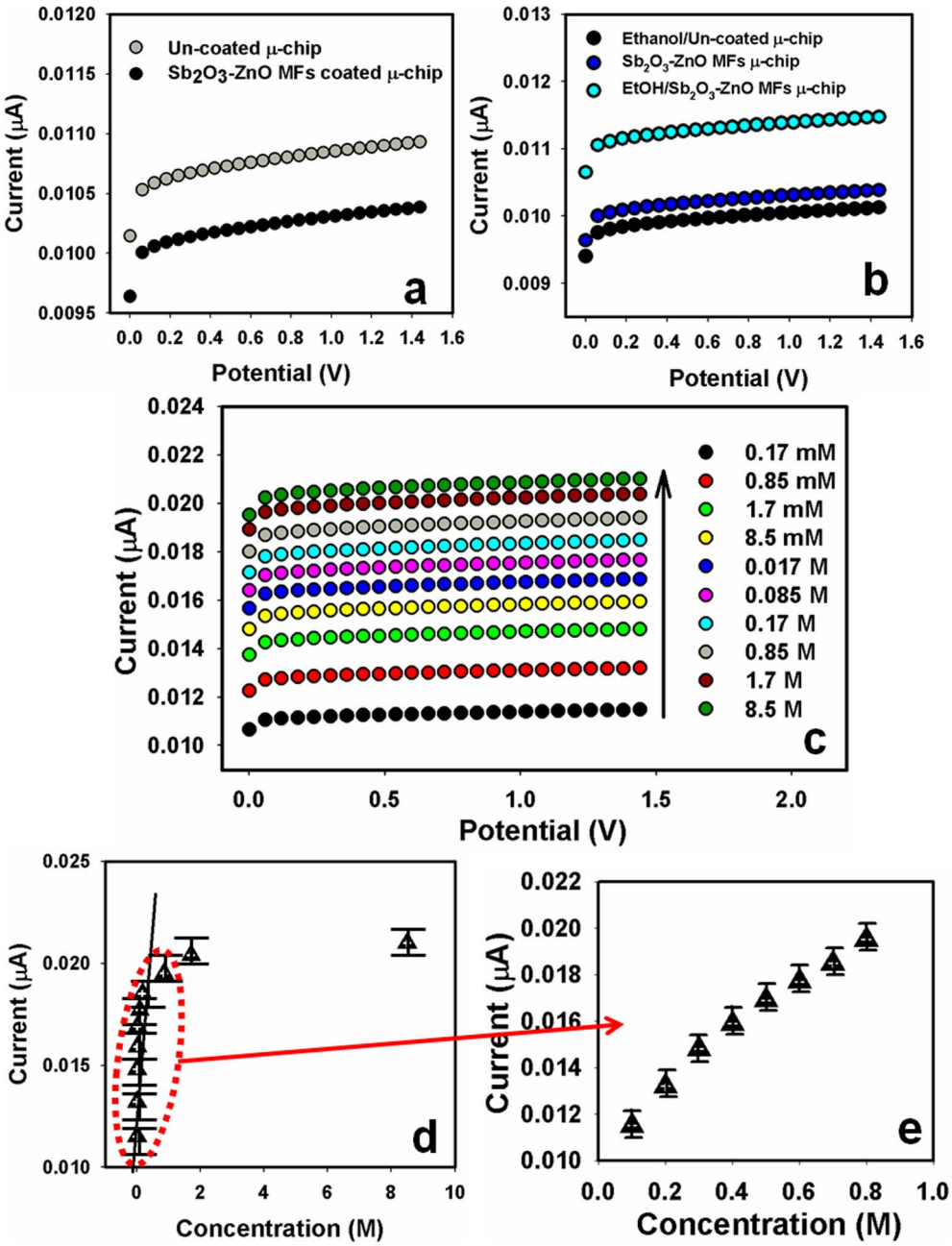

Figure 5. I–V responses of (a) un-coated and Sb_2O_3-ZnO MFs coated μ-chip without ethanol; (b) with 0.17 mM ethanol for un-coated μ-chip; without ethanol for Sb_2O_3-ZnO MFs coated μ-chip; and with 0.17 mM ethanol for Sb_2O_3-ZnO MFs coated μ-chip; (c) concentration variations (0.17 mM to 8.5 M) of analyte; and (d) calibration plot of doped nanomaterial fabricated on μ-chip surfaces. Potential was chosen in 0.1 to +1.4 V ranges. Error limit of I-V measurement was ± 0.001. There are three trial has been done in same experimental concentration at similar condition. Coefficient variation (CV): 0.1699.
doi:10.1371/journal.pone.0085036.g005

$$\mathbf{O_{2(diss)}}\ (Sb_2O_3-ZnO\ MFs/\mu\text{-chip}) \rightarrow \mathbf{O_{2(ads)}} \quad \textbf{(vi)}$$

$$\mathbf{e^-}\ (Sb_2O_3-ZnO\ MFs/\mu\text{-chip})+\mathbf{O_2} \rightarrow \mathbf{O_2^-} \quad \textbf{(vii)}$$

$$\mathbf{e^-}\ (Sb_2O_3-ZnO\ MFs/\mu\text{-chip})+\mathbf{O_2^-} \rightarrow \mathbf{2O^-} \quad \textbf{(viii)}$$

These reactions are held in bulk-system or air/liquid interface or adjacent atmosphere due to the small carrier concentration which enhanced the resistances. The ethanol sensitivity could be attributed to the high oxygen deficiency on Sb_2O_3-ZnO MFs/μ-chip (eg. MO_x) and higher density conducts to increase oxygen adsorption. Larger the quantity of oxygen adsorbed on the fabricated sensor surface, larger would be the oxidizing potential as well as faster would be the oxidation of ethanol. The reactivity of ethanol would have been very large as compared to other fabricated material surfaces surface under identical condition [61–63]. When ethanol reacts with the adsorbed oxygen on the exterior/interior of the Sb_2O_3-ZnO MFs/μ-chip layer, it oxidized to carbon dioxide and water by releasing free electrons ($6e^-$) in the

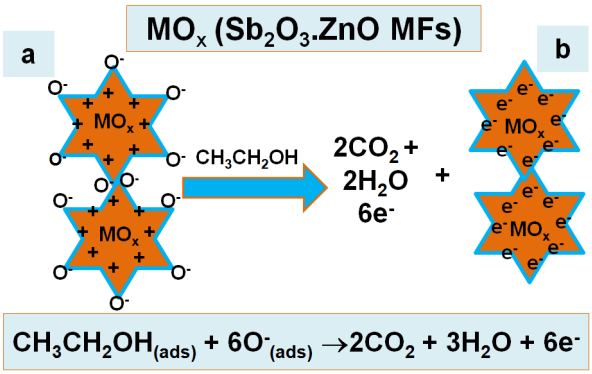

Figure 6. Mechanism of Sb_2O_3-ZnO MFs/μ-chip ethanol chemical sensors at ambient conditions.
doi:10.1371/journal.pone.0085036.g006

conduction band, which is expressed through the following reactions (ix).

$$\mathbf{CH_3CH_2OH_{(ads)}+6O^-_{(ads)} \rightarrow 2CO_2+3H_2O+6e^-(C.B.)\ (ix)}$$

In the reaction system, these reactions referred to oxidation of the reducing carriers. This method is enhanced the carrier concentration and consequently decreased the resistance on adjacent reducing analytes. The elimination of ionosorbed oxygen amplified the electron concentration onto Sb_2O_3-ZnO MFs/μ-chip and hence the surface conductance is increased in the film [64,65]. The reducing analyte (ethanol) gives electrons to Sb_2O_3-ZnO MFs/μ-chip surface. Consequently, resistance is reduced, and hence the conductance is increased. This is the cause why the analyte response (current) amplifies with increasing potential. Thus produced electrons contribute to rapid increase in conductance of the thick Sb_2O_3-ZnO MFs/μ-chip film. The Sb_2O_3-ZnO MFs unusual regions dispersed on the surface would progress the capability of nanomaterial to absorb more oxygen species giving high resistance in air ambient, which is presented in Figure 6.

On the other approach, the utmost ethanol response of Sb_2O_3-ZnO MFs/μ-chip was attributed to the larger chemical communication on the sensing surface due to the larger surface area and meso-porous natures. The high ethanol response of the Sb_2O_3-ZnO MFs can be understandable in more detail in relative to the probable chemical-sensing mechanism, in terms of p-type doped semiconductor nano-materials. The oxide surface of an p-type semiconductor is readily covered with chemisorbed oxygen [66,67]. Therefore, at identical condition, the adsorption of negatively charged oxygen can generate the holes for conduction. The subsequent ethanol-sensing reactions might be considered according to the charges of the adsorbed oxygen species (Sb_2O_3-ZnO MFs/μ-chip) under the statement of full oxidation of C_2H_5OH according to the following equations (x-xi).

$$\mathbf{^1/_2O_{2(g/l)} \leftrightarrow O^-_{(ads)}\ (Sb_2O_3-ZnO\ MFs/\mu-chip)+h^\circ\ (x)}$$

$$\mathbf{C_2H_5OH_{(g)}+6O^-_{(ads)}+6h^\circ \rightarrow 2CO_{2(g)}+3H_2O_{(g)}\ (xi)}$$

The oxidation reaction with reducing ethanol amplifies the resistivity of the surface regions of the p-type doped Sb_2O_3-ZnO MFs/μ-chip, which in turn enhances the sensor resistance. The resistive contacts among the Sb_2O_3-ZnO MFs nano-materials control the chemi-sensor resistance. Therefore, the ethanol response is extensively dependent upon the dimensions of the nano-sheet composed MFs, the large-active surface area and the nano-porosity. According to the charge accumulation reproduction of p-type semiconductors, the conduction occurs along the conductive as well as active sensor surface of Sb_2O_3-ZnO MFs/μ-chip [68–70].

The sensor response time was ~10.0 sec for the Sb_2O_3-ZnO MFs coated μ-chip sensor to achieve saturated steady state current in I–V plots. The major sensitivity of μ-chip sensor can be attributed to the good absorption (porous surfaces MFs fabricated with binders), adsorption ability, high-catalytic activity, and good bio-compatibility of the Sb_2O_3-ZnO MFs/μ-chip. The expected sensitivity of the MF fabricated sensor is relatively better than previously reported ethanol sensors based on other composites or materials modified electrodes [71]. Due to perceptive surface area, here the doped nano-materials proposed a beneficial microenvironment for the toxic chemical detection (by adsorption) and recognition with excellent quantity. The prominent sensitivity of Sb_2O_3-ZnO MFs affords high electron communication features which improved the direct electron communication between the active sites of nano-sheets composed microstructures and μ-chips. The modified thin Sb_2O_3-ZnO MFs/μ-chip sensor film had a better reliability as well as stability in ambient conditions. Sb_2O_3-ZnO MFs/μ-chip exhibits several approaching in providing ethanol chemical based sensors, and encouraging improvement has been accomplished in the research section.

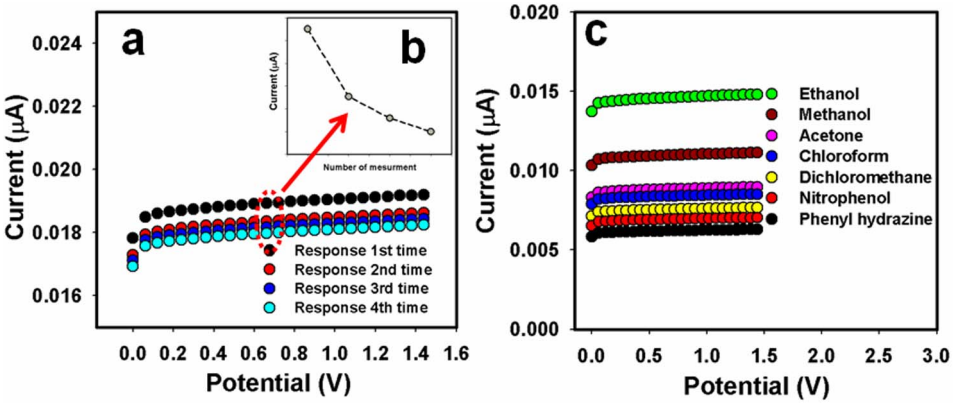

Figure 7. I–V responses of Sb_2O_3-ZnO MFs coated μ-chip are presented for ethanol sensors reproducibility (a), sensor-responses (inset, b), and selectivity (c) study. Ethanol and other chemicals concentration are taken as1.0 mM for selectivity study.
doi:10.1371/journal.pone.0085036.g007

Table 1. Comparison the performances for ethanol detection based on various nanomaterial fabricated electrodes.

Materials	Methods	Linear Dynamic Range, LDR	Sensitivity	Linearity, r^2	Limit of Detection, LOD	Response Time	References
Ni/Pt/Ti	Potential amperometry	–	3.08 $\mu AmM^{-1}\ cm^{-2}$	–	–	–	[72]
Ni-doped SnO_2 nanostructure	I–V	1.0 nM~1.0 mM	2.3148 $\mu A\ cm^{-2}mM^{-1}$	0.8440	0.6 nM	10.0 s	[73]
Pd–Ni/SiNWs electrode	Potential amperometry	–	0.76 $mAmM^{-1}cm^{-2}$	0.9970	10.0 μM	–	[74]
ZnO-CeO_2 Nanoparticles	I–V	1.7 mM~1.7 M	2.1949 $\mu A\ cm^{-2}mM^{-1}$	0.9463	0.6± 0.05 mM	10.0 s	[75]
RuO-modified Ni electrode	Cyclic voltammetry	100~1000 ppm	4.92 $\mu Appm^{-1}cm^{-2}$	–	–	13.0 s	[76]
CeO_2 nanoparticles	I–V	0.17 mM~0.17 M	0.92 $\mu Acm^{-2}mM^{-1}$	0.7458	0.124±0.010 mM	10.0 s	[77]
Al-doped ZnO nanomaterial	I–V method	Up to 3000 ppm	1000 ppm ethanol	–	–	~8.0 s	[78]
CuO nanosheets	I–V	up to 1.7 M	~0.9722 $\mu Acm^{-2}mM^{-1}$	0.7806	0.143 mM	10.0 s	[79]
Sm-Doped Co_3O_4 Nanokernels	I–V	1.0 nM~10.0 mM	2.1991±0.10 $\mu Acm^{-2}mM^{-1}$	0.9065	0.63±0.02 nM	10.0 s	[80]
Sb_2O_3-ZnO MFs	**I–V**	**0.17 mM~0.85 M**	**5.845 uA $cm^{-2}mM^{-1}$**	**0.9989**	**0.11 ±0.02 mM**	**10.0 s**	**Current work**

doi:10.1371/journal.pone.0085036.t001

To check the reproducibly and storage stabilities, I–V response for Sb_2O_3-ZnO MFs coated μ-chip sensor was examined (up to 2 weeks). After each experiment, the fabricated Sb_2O_3-ZnO MFs/μ-chip substrate was washed thoroughly with the PBS buffer solution and observed that the current response was not significantly decreased (Figure 7a). The sensitivity was retained almost same of initial sensitivity up to week (1^{st} to 2^{nd} week), after that the response of the fabricated electrode gradually decreased. A series of six successive measurements of 0.17 mM ethanol in 0.1 mM PBS yielded a good reproducible signal at Sb_2O_3-ZnO MFs/μ-chip sensor in different conditions with a relative standard deviation (RSD) of 3.7% (Figure not shown). The sensor-to-sensor and run-to-run repeatability for 0.17 mM ethanol detection were found to be 1.9% using Sb_2O_3-ZnO MFs/μ-chip. To investigate the long-term storage stabilities, the response for the MFs sensor was determined with the respect to the storing time. The long-term storing stability of the Sb_2O_3-ZnO MFs/μ-chip sensor was investigated significantly at room conditions. The sensitivity retained 94% of initial sensitivity for several days. The above results clearly suggested that the fabricated sensor can be used for several weeks without any significant loss in sensitivity. The dynamic response (0.17 mM to 0.85 M) of the sensor was investigated from the practical concentration variation curve. The sensor response time is mentioned and investigated using this sensor system at room conditions. In this study, it shows the MFs/Chips-based ethanol sensor response after successive injection in buffer solutions containing 1.0 mM of ethanol, which is presented in Figure 7a. A recovery time is observed with a small loss of signal (~0.007uA), suggesting that the sensor can be re-used further [Figure 7b (inset)]. It was also investigated the sensing selectivity performances (interferences) with other chemicals like methanol, acetone, chloroform, dichloromethane, phenyl hydrazine, nitrophenol etc. Ethanol exhibited the maximum current response by I–V system using MFs fabricated micro-chip electrode compared to methanol and others. It was specific towards ethanol compared to all other chemicals. A comparative study with all chemicals using Sb_2O_3-ZnO MFs/μ-chip is included in Figure 7c. In Table 1, it is compared the performances for ethanol chemical detection based Sb_2O_3-ZnO MFs/μ-chip using various modified electrode materials [72–80].

Conclusion

Transition-metal doped semiconductor Sb_2O_3-ZnO MFs are prepared by easy, simple, efficient, reliable, and economical approaches using reducing agents. The structural, morphological, and optical properties are performed by using XRD, XPS, FE-SEM, and UV-visible techniques respectively. The Sb_2O_3-ZnO MFs/μ-chip has assembled by simple fabricated method and displayed higher sensitivity for chemical sensing. They are efficiently prepared for sensitive ethanol sensor based on Sb_2O_3-ZnO MFs embedded μ-chips with conducting coating binders, for the first time. The analytical performances of the fabricated ethanol MFs sensors are excellent in terms of sensitivity, detection limit, linear dynamic ranges, and in short response time. Sb_2O_3-ZnO MFs/μ-chips are exhibited higher-sensitivity (~5.845uA $cm^{-2}mM^{-1}$) and lower-detection limit (~0.11±0.02 mM) with good linearity in short response time, which efficiently utilized as chemi-sensor for ethanol onto μ-chips. This novel attempt is introduced a well-organized route of efficient chemical sensor development for environmental toxic pollutants and health-care fields in broad scale.

Acknowledgments

This work was funded by the Deanship of Scientific Research (DSR), King Abdulaziz University, Jeddah, under grant No. **130-019-D1433**. The authors, therefore, acknowledge with thanks DSR technical and financial support.

Author Contributions

Conceived and designed the experiments: MMR. Performed the experiments: MMR SBK. Analyzed the data: MMR SBK AMA. Contributed reagents/materials/analysis tools: MMR SBK AMA. Wrote the paper: MMR.

References

1. Kumar A, Singhal A (2007) Synthesis of colloidal β-Fe_2O_3 nanostructures-influence of addition of Co^{2+} on their morphology and magnetic behavior. Nanotechnol 18: 475703-475710.
2. Whitesides GM, Boncheva M (2002) Beyond molecules: Self-assembly of mesoscopic and macroscopic components. Proc Natl Acad Sci USA. 99: 4769–4774.
3. Dale L, Huber (2009) Synthesis, properties, and applications of iron NPs. Small 1: 482–501.
4. Shaalan NM, Yamazaki T, Kikuta T (2011) Influence of morphology and structure geometry on NO_2 gas-sensing characteristics of SnO_2 nanostructures synthesized via a thermal evaporation method. Sens Actuator B 153: 11–16.
5. Rahman MM, Jamal A, Khan SB, Faisal M, Asiri AM (2012) Highly Sensitive methanol chemical sensor based on undoped silver oxide nanoparticles prepared by a solution method. Microchim Acta 178: 99–106.
6. Umar A, Rahman MM, Kim SH, Hahn YB (2008) Zinc oxide nanonail based chemical sensor for hydrazine detection. Chem Commun 166–169.
7. Rahman MM, Jamal A, Khan SB, Faisal M (2011) Characterization and applications of as-grown β-Fe_2O_3 nanoparticles prepared by hydrothermal method. J Nanopart Res 13: 3789–3799.
8. Yao C, Zeng Q, Goya GF, Torres T, Liu J, et al (2007) $ZnFe_2O_4$ nanocrystals: synthesis and magnetic properties. J Phys Chem C 111: 12274–12278.
9. Ingler-Jr WB, Baltrus JP, Khan SUM (2004) Photoresponse of p-Type Zinc-Doped Iron(III) Oxide Thin Films. J Am Chem Soc 126: 10238–10239.
10. Holmes JD, Johnston KP, Doty RC, Korgel BA (2000) Control of Thickness and Orientation of Solution-Grown Silicon Nanowires. Science 287: 1471–1473.
11. Pan Z, Dai Z, Wang ZL (2001) Nanobelts of semiconducting oxides. Science 291: 1947–1949.
12. Wang N, Tang Y, Zhang Y, Lee CS, Lee ST (1998) Nucleation and growth of Si nanowires from silicon oxide. Phys. Rev. B 58: R16024–R16026.
13. Gui L, Wu Z, Liu T, Wang W, Zhu H (2000) Synthesis of novel Sb_2O_3 and Sb_2O_5 nanorods. Chem. Phys. Lett. 318: 49.
14. Friedrichs S, Meyer RR, Sloan J, Kirkland AI, Hutchison JL, et al (2001) Complete characterisation of a Sb_2O_3/(21,−8)SWNT inclusion composite. Chem. Commun. 929–930.
15. Suchea M, Christoulakis S, Katsarakis N, Kitsopoulos T, Kiriakidis G (2007) Comparative study of zinc oxide and aluminium doped zinc oxide transparent thin films by direct current magnetron sputtering. Thin Sol Film 515: 6562.
16. Lee SR, Rahman MM, Ishida M, Sawada K (2009) Development of highly sensitive acetylcholine sensor based on acetylcholine by charge transfer techniques esterase using smart biochips. Trends Anal Chem 28: 196.
17. Pearton SJ, Heo WH, Ivill M, Norton DP, Steiner T (2004) Dilute magnetic semiconducting oxides. Semicond Sci Technol 19:59.
18. Nomura K, Ohta H, Ueda K, Kamiya T, Hirano M, et al (2003) Thin-film transistor fabricated in single-crystalline transparent oxide semiconductor. Science 300: 1269.
19. Umar A, Rahman MM, Vaseem M, Hahn YB (2009) Ultra-Sensitive Cholestrol Biosensor Based on Low Temperature Grown ZnO Nanoparticles. Electrochem. Commun. 11: 118
20. Rahman MM, Jamal A, Khan SB, Faisal M (2011) CuO Codoped ZnO Based Nanostructured Materials for Sensitive Chemical Sensor Applications. ACS Appl Mater Interfac 3: 1346.
21. Wang ZLJ (2004) Zinc oxide nanostructures: growth, properties and applications. Phys Condens Matt 16: 829.
22. Ng HT, Han J, Yamada T, Nguyen P, Chen YP, et al (2004) Single Crystal Nanowire Vertical Surround-Gate Field-Effect Transistor. Nano Lett 4: 1247.
23. Soci C, Zhang A, Xiang B, Dayeh SA, Aplin DPR, et al (2007) ZnO Nanowire UV Photodetectors with High Internal Gain. Nano Lett 7: 1003.
24. Lee SR, Rahman MM, Ishida M, Sawada K (2009) Fabrication of a Highly Sensitive Penicillin Sensor Based on Charge Transfer Techniques. Biosens Bioelectron 24: 1877.
25. Huang MH, Mao S, Feick H, Yan H, Wu Y, et al (2001) Room temperature ultraviolet nanowire nanolasers. Science 292: 1897.
26. Wang XD, Song JH, Liu J, Wang ZL (2007) Direct-Current Nano-generator Driven by Ultrasonic Waves. Science 316: 102.
27. Lee SR, Rahman MM, Ishida M, Sawada K (2009) Development of highly sensitive acetylcholine sensor based on acetylcholine by charge transfer techniques esterase using smart biochips. Trends in Anal. Chem. 28: 196–203.
28. Khan SB, Rahman MM, Jang ES, Akhtar K, Han H (2011) Special susceptive aqueous ammonia chemi-sensor: Extended applications of novel UV-curable polyurethane-clay nanohybrid. Talanta 84: 1005–1010.
29. Yang Z, Huang Y, Chen G, Guo Z, Cheng S, et al (2009) Ethanol gas sensor based on Al-doped ZnO nanomaterial withmany gas diffusing channels. Sens Actuator B Chem 140: 549–556.
30. Gonga H, Hu JQ, Wang JH, Ong CH, Zhu FR (2006) Nano-crystalline Cu-doped ZnO thin film gas sensor for CO. Sens Actuator B: Chem 115: 247–251.
31. Francesco FD, Fuoco R, Trivella MG, Ceccarini A (2005) Breath analysis:trends in techniques and clinical applications. Microchem J 79: 405.
32. GW, Park KY, Anwar MS, Seo YJ, Sung CH, et al (2012) Preparation and properties of Sb_2O_3-doped SnO_2 thin films deposited by using PLD. J Kor Phys Soc 60: 1548–1551.
33. Mori H, Sakata H (1996) Oxygen gas-sensing properties of V_2O_5-Sb_2O_3-TeO_2 glass. Materials Chemistry and Physics 45: 211–215.
34. Montenegro A, Ponce MA, Castro MS, Rodríguez-Paez JEJ (2007) SnO_2-Bi_2O_3 and SnO_2-Sb_2O_3 gas sensors obtained by soft chemical method. J European Ceram Soc 27: 4143–4146.
35. Rahman MM, Umar A, Sawada K (2009) Development of Amperometric Glucose Biosensor Based on Glucose Oxidase Enzyme Immobilized with Multi-Walled Carbon Nanotubes at Low Potential. Sens Actuator B 137: 327–333.
36. Nicoletti S, Zampolli S, Elmi I, Dori L, Severi M (2003) Use of different sensing materials and deposition techniques for thin-film sensors to increase sensitivity and selectivity. IEEE Sens J 3: 454–459.
37. Aguilar-Leyva A, Maldonado, De-la-Olvera M (2007) Gas-sensing characteristics of undoped-SnO2 thin films and Ag/SnO2 and SnO2/Ag structures in a propane atmosphere. Mater Character 58: 740–744.
38. Zhang C, Hu Y, Lu W, Cao M, Zhou D (2002) Influence of TiO_2/Sb_2O_3 ratio on ZnO varistor ceramics. J Europ Ceram Soc 22: 61–65.
39. Das S, Kim DY, Choi CM, Hahn YB (2011) Influence of aqueous hexamethylenetetramine on the morphology of self-assembled SnO_2 nanocrystals. Mater Res Bull 46: 609–614.
40. Lao YW, Kuo ST, Tuan WH (2007) Effect of Bi_2O_3 and Sb2O3 on the grain size distribution of ZnO. J. Electroceram. 19: 187–194.
41. Vicente FSD, Li MS, Nalin M, Messaddeq Y (2003) Photoinduced structural changes in antimony polyphosphate based glasses. J. Non-Crystall. Sol. 330: 168–173.
42. Han N, Chai L, Wang Q, Tian Y, Deng P, et al (2010) Evaluating the doping effect of Fe, Ti and Sn on gas sensing property of ZnO. Sens Actuator B Chem 147: 525–530.
43. Gibert JP, Cuesta JML, Bergeret A, Crespy A (2000) Study of the degradation of fire-retarded PP/PE copolymers using DTA/TGA coupled with FTIR. Poly Degrad Stability 67: 437–447.
44. Li Y, Yi R, Yan A, Deng L, Zhou K, et al (2009) Facile synthesis and properties of $ZnFe_2O_4$ and $ZnFe_2O_4$/polypyrrole core-shell nanoparticles. Sol Stat Sci 11: 1319–1324.
45. Damen TC, Porto SPS, Tell B (1966) Raman-effect in zinc oxide. Phys Rev 142: 570–574.
46. Rahman MM, Khan SB, Faisal M, Asiri AM, Tariq M A (2012). Detection of Aprepitant Drug Based on Low-dimensional Un-doped Iron oxide Nanoparticles Prepared by Solution method. Electrochim. Acta 75: 164–170.
47. Bundesmann C, Ashkenov N, Schubert M, Spemann D, Butz T, et al (2003) Raman scattering in ZnO thin films doped with Fe, Sb, Al, Ga, and Li. Appl Phys Lett 83: 1974–1976.
48. Cebriano T, Méndez B, Piqueras J (2012) Micro- and nanostructures of Sb_2O_3 grown by evaporationedeposition: Self assembly phenomena, fractal and dendritic growth. Mater Chem Phys 135: 1096–1103.
49. Rahman MM, Jamal A, Khan SB, Faisal M (2011) Characterization and Applications of as-grown β-Fe_2O_3 Nanoparticles Prepared by Hydrothermal Method. J Nanopart Res 13: 3789–3799.
50. Rahman MM, Khan SB, Faisal M, Asiri AM, Alamry KA (2012) Highly Sensitive Formaldehyde Chemical Sensor Based on Hydrothermally Prepared Spinel $ZnFe_2O_4$ Nanorods. Sens Actuator B: Chem 171–172: 932–937.
51. Umar A, Rahman MM, Kim SH, Hahn YB (2008) ZnO Nanonails: Synthesis and Their Application as Glucose Biosensor. J Nanosci Nanotech 8: 3216.
52. Faisal M, Khan SB, Rahman MM, Jamal A, Asiri AM, Abdullah MM (2012) Fabrication of ZnO nanoparticles based sensitive methanol sensor and efficient photocatalyst. App Surf Sci 258: 7515–7522.
53. Khan SB, Faisal M, Rahman MM, Jamal A (2011) Low-temperature Growth of ZnO Nanoparticles: Photocatalyst and Acetone Sensors. Talanta 85: 943–949.
54. Jamal A, Rahman MM, Faisal M, Khan SB (2011) Studies on Photocatalytic Degradation of Acridine Orange and Chloroform Sensing Using As-Grown Antimony Oxide Microstructures. Mater Sci Appl 2: 676–683.
55. Ye C, Meng G, Zhang L, Wang G, Wang Y (2002) A facile vapor–solid synthetic route to Sb_2O_3 fibrils and tubules. Chem Phys Lett 363: 34–38.
56. Rahman MM, Khan SB, Faisal M, Rub MA, Al-Youbi AO, et al (2012) Determination of Olmisartan medoxomil using hydrothermally prepared nanoparticles composed SnO_2-Co_3O_4 nanocubes in tablet dosage forms. Talanta 99: 924–931.

57. Fujii T, de-Groot FMF, Sawatzky GA, Voogt FC, Hibma T, et al (1999) Phys Review B 59: 3195–3202.
58. Rahman MM (2011) Fabrication of Mediator-free Glutamate Sensors Based on Glutamate Oxidase using Smart Micro-devices. J Biomed Nanotech 7: 351–357.
59. Song P, Qin HW, Zhang L, An K, Lin ZJ, et al (2005) The structure, electrical and ethanol-sensing properties of La1−xPbxFeO3 perovskite ceramics with x≤ 0.3. Sens Actuator B: Chem 104: 312–316.
60. Hsueh TJ, Hsu CL, Chang SJ, Chen IC (2007) Laterally grown ZnO nanowire ethanol gas sensors. Sens Actuator B Chem. 126: 473–477.
61. Tao B, Zhang J, Hui S, Wan L (2009) An amperometric ethanol sensor based on a Pd–Ni/SiNWs electrode. Sens Actuator B Chem142: 298–303.
62. Wongrat E, Pimpang P, Choopun S (2009) Comparative study of ethanol sensor based on gold nanoparticles: ZnO nanostructure and gold: ZnO nanostructure. App Surf Sci 256: 968–971.
63. Rahman MM, Jamal A, Khan SB, Faisal M (2011) Fabrication of chloroform sensors based on hydrothermally prepared low-dimensional β-Fe_2O_3 nanoparticles. Superlatt Microstruc 50: 369–376.
64. Mujumdar S (2009) Synthesis and characterization of SnO_2 films obtained by a wet process. Mat Sci Poland 27: 123.
65. Rahman MM, Jamal A, Khan SB, Faisal M, Asiri AM (2011) Fabrication of Phenyl-Hydrazine Chemical Sensor based on Al-doped ZnO Nanoparticles. Sens Transduc J 134: 32–44.
66. Hagen J (1999) Heterogeneous Catalysis: Fundamentals, Wiley-VCH, Weinheim, 83–206.
67. Rahman MM, Jamal A, Khan SB, Faisal M, Asiri AM (2012) Fabrication of Highly Sensitive Acetone Sensor Based on Sonochemically Prepared As-grown Ag_2O Nanostructures. Chem Engineer J 192: 122–128.
68. Sahner K, Moos R, Matam M, Tunney JJ (2005) Hydrocarbon sensing with thick and thin film p-type conducting perovskite materials, Sens. Actuator. B 108: 102–112.
69. Pokrel S, Simon CE, Quemener V, Bârsan N, Weimer U (2008) Investigation of conduction mechanism in Cr_2O_3 gas sensing thick films by ac impedance spectroscopy and work function changes measurements, Sens Actuator B: Chem 133: 78–83.
70. Wang C, Fu XQ, Xue XY, Wang YG, Wang TH (2007) Surface accumulation conduction controlled sensing characteristics of p-type CuO nanorods induced by oxygen adsorption, Nanotech. 18: 145506.
71. Choi KI, Kim HR, Kim KM, Liu D, Cao G, et al (2010) C_2H_5OH sensing characteristics of various Co_3O_4 nanostructures prepared by solvothermal reaction. Sens Actuator B: Chem 146: 183–189.
72. Weng YC, Rick JF, Chou TC (2004) A sputtered thin film of nanostructured Ni/Pt/Ti on Al_2O_3 substrate for ethanol sensing, Biosens Bioelectron 20: 41–51.
73. Rahman MM, Jamal A, Khan SB, Faisal M (2011) Highly sensitive ethanol chemical sensor based on Ni-doped SnO_2 nanostructure Materials. Biosens Bioelectron 28: 127–134
74. Tao B, Zhang J, Hui S, Wan L (2009) An amperometric ethanol sensor based on a Pd-Ni/SiNWs electrode. Sens Actuator B Chem. 142: 298–303.
75. Faisal M, Khan SB, Rahman MM, Jamal A, Asiri AM, et al (2011) Smart chemical sensor and active photo-catalyst for environmental pollutants. Chem Engineer J 173:178–184.
76. Weng YC, Chou TC (2002) Ethanol sensors by using RuO_2-modified Ni electrode. Sens Actuator B Chem 85: 246–255.
77. Khan SB, Faisal M, Rahman MM, Jamal A (2011) Exploration of CeO_2 nanoparticles as a chemi-sensor and photo-catalyst for environmental applications. Sci Total Environ 409: 2987–2992.
78. Yang Z, Huang Y, Chen G, Guo Z, Cheng S, et al (2009) Ethanol gas sensor based on Al-doped ZnO nanomaterial with many gas diffusing channels. Sens Actuator B Chem 140: 549–556.
79. Faisal M, Khan SB, Rahman MM, Jamal A, Umar A (2011) Ethanol chemi-sensor: Evaluation of structural, optical and sensing properties of CuO nanosheets. Mater Lett 65: 1400–1403.
80. Rahman MM, Jamal A, Khan SB, Faisal M (2011) Fabrication of Highly Sensitive Ethanol Chemical Sensor Based on Sm-Doped Co_3O_4 Nanokernels by a Hydrothermal Method. J Phys Chem C 115: 9503–9510.